Onset of sidebranching in directional solidification

M. Georgelin and A. Pocheau
Institut de Recherche sur les Phénomènes Hors Equilibre, S.252, Université Saint-Jérome, 13397 Marseille, France
(Received 24 October 1996; revised manuscript received 18 November 1997)

We study the onset of sidebranching of growth cells in directional solidification of impure succinonitrile. Care is taken to obtain uniform cell spacing over large distances in order to use this variable as a true control parameter. Two sidebranching modes referring to different crystalline orientations are observed and their physical equivalence is shown. The onset of sidebranching is identified according to an order parameter and scanned with respect to pulling velocity, thermal gradient, and cell spacing. Its evolution with the control parameters surprisingly reveals that increasing thermal gradient at otherwise fixed velocity and cell spacing enhances sidebranching. These results show the need for improving the experimental characterization and the theoretical description of sidebranching in directional solidification. [S1063-651X(98)04803-X]

PACS number(s): 68.70.+w, 81.30.Fb, 47.20.Hw

I. INTRODUCTION

In the past decade, considerable attention has been given to the origin of dynamics in out-of-equilibrium systems. In particular, most of the mechanisms responsible for primary or secondary instabilities in pattern forming systems have been identified, at least qualitatively [1]. However, despite considerable progress, one remains unsatisfactorily understood. It consists in the repetitive generation of sidebranches on the growth forms appearing during the solidification of crystals (Fig. 1) [2,3].

Evidence of sidebranching emissions extends to different kinds of growth: unlimited free growth [4–8], free growth confined to a channel [9], or directional growth [10–15]. In the former case, many improvements have been made to a noise-amplification theory [4,16–20] proposed by analogy with curved flame fronts [21]. They revealed a highly sensitive dependence of sidebranching on growth forms [22,23], which contrasts with the uncertainty prevailing at present as to the branch of solutions relevant to confined free growth [9,24–27] or directional growth [24,28]. On the other hand, some evidence of larger than usual correlation of sidebranch emissions [10,29] raises questions as to the universality or relevance of a noise-induced mechanism. Further investigations seem therefore necessary, in particular in directional growth, to draw a conclusion on the nature of the sidebranching mechanism: a noise-amplification phenomenon [30] or a nonlinear global mode [31].

This alternative depends on whether cells emitting sidebranches behave as noise amplifiers or as oscillators. In the former case, their dynamics is extrinsic since it is controlled by noisy excitations; in the latter case, it is intrinsic since it corresponds to an attractor of the dynamic system whose main features do not refer to noise. We notice that the same problem actually arises in another kind of advective system, the hydrodynamics of open flows, since mixing layers and flat-plate wakes induce noise amplification whereas bluff-body wakes and hot-density jets generate oscillations [32]. On this topic, the alternative has been linked to the convective or absolute nature of unstable linear modes: convective instabilities imply noise amplification but absolute instability may yield nonlinear global modes [33] if perturbations withstand advection. In crystal growth, the latter property is conditioned by the shapes of the growth states undergoing sidebranching. We review them below in different kinds of growth.

In unlimited free growth, crystal shapes are shown to depend sensitively on surface tension and crystalline anisotropy, which act as singular perturbations [22]. Then the degeneracy of the family of solutions deduced by dimensionality, the Ivantsov paraboloids [34], is removed and anisotropic needle crystals close to, but different from, paraboloids are selected. The extrinsic scenario proposed for sidebranching then consists in a selective amplification of localized thermal disturbances in the course of their propagation down the side of the needle crystal. One of its striking feature is a large sensitivity to the shape of the growth interface: for paraboloids, the amplification of thermal noise is too weak to fit with observations [18]; for nonaxisymmetric needle crystals, it is sufficient to explain the observed amplitudes of sidebranches [23].

In confined free growth, the situation is complicated by the occurrence of two branches of solutions at given undercooling Δ, channel width Λ, and anisotropy α [27]. One of them, the Saffman-Taylor (ST) branch, has been derived at low Péclet number $\mathrm{Pe}=\Lambda V/D$, by analogy with viscous fin-

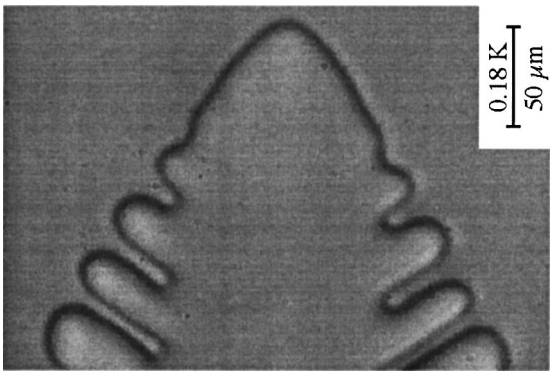

FIG. 1. Enlarged view of a cell emitting sidebranches in directional solidification, far from the sidebranching onset. Pulling velocity $V=24\ \mu$m/s, planar critical velocity $V_c=0.75\ \mu$m/s, cell width $\Lambda=260\ \mu$m, view width 270 μm.

gering, D being the solutal diffusivity and V the growth velocity [24]. It is characterized by a decrease of velocity with Δ, $(\partial V/\partial\Delta)_\Lambda<0$, which contrasts with the increase, $(\partial V/\partial\Delta)_\Lambda>0$, displayed in unlimited free growth. This irreducible difference raises the problem of asymptotic matching going from confined to unlimited free growth as $\Lambda\to\infty$. It has been solved by the identification by Brener, Geilikman, and Temkin of another branch of solution characterized by $(\partial V/\partial\Delta)_\Lambda>0$, the so-called dendrite branch, which merges with the solution of unlimited free growth in the limit $\Lambda\to\infty$ [27]. These branches, the ST branch at a moderate Péclet number and the dendrite branch at a large Péclet number, might correspond to the cell forms observed by Molho, Simon, and Libchaber [9]. Following a numerical prediction [26], these authors nevertheless noticed an unsteadiness of the crystal shape in the low Péclet number regime, which has further been explained by an instability of the ST branch at low Péclet numbers [25]. Despite this instability, the question of the nature of the branch of solution at a moderate Péclet number remains. In view of the sensitivity of noise amplification to the crystal shape, this greatly complicates the understanding of sidebranching in this kind of growth. On the other hand, we notice that, in contrast with unlimited free growth, a threshold for sidebranching is displayed in practice [9]. It is unclear whether it is due to a change of branch or to an instability of a definite branch [9].

The last kind of growth is directional growth, in which a melt is forced to solidify at a given velocity V within a thermal gradient G. Here the ST branch of solutions remains and is stabilized by the thermal gradient [35]. The relevance of this branch, however, is questioned by Weeks and Van Saarloos [28] for different reasons. One of the reasons is that, in the experimental regime of a moderate Péclet number and low effective surface tension, the ST branch implies wide grooves in contrast with the narrow ones observed experimentally [13]. Another reason is that, to satisfactorily approximate cells by the ST profile, an effective surface tension that is one order of magnitude larger than expected is required [13]. Both mean that the ST branch may capture the cell shape, but for unexpected physical parameters. Here too, this ambiguity regarding the branch of solution relevant to cellular growth obscures the interpretation of sidebranching: on one hand, noise amplification is in agreement with the response of cells to imposed noise [14] but has not been derived on actual cellular profiles; on the other hand, the ST branch of solution shows an example of an intrinsic oscillatory instability [35] qualitatively similar to a vacillating-breathing instability recently observed on cell pairs [36]. As this instability relies on tip oscillations that have never been observed on sidebranching cells [10–15], it cannot be taken to be a possible mechanism for sidebranching. Yet, it stresses that the nature, extrinsic or intrinsic, of the dynamical mechanisms involved in cellular growth crucially depends on the detailed features of cellular forms.

The present study addresses the sidebranching phenomenon in directional solidification from an experimental point of view. According to the above statements, the branch of solution actually followed by growth cells appears of primary importance to the sidebranching mechanism. However, determining it appears problematic in practice, since the analytical expressions of the geometry of the possible branches of solutions in the experimental regime of moderate Péclet numbers is unknown at the level of accuracy required to decide among them. A possibility would be to indirectly investigate the branch of solution, for instance, from the temperature or the curvature radius of cell tips, but this would not fully characterize the cellular state anyway. To improve understanding of sidebranching, we have thus chosen to adopt a different strategy. It consists in indirectly characterizing the sidebranching phenomenon itself by following its *onset* in the control parameter space of directional growth. We thus obtain relevant information on sidebranching while by-passing the determination of cellular form. In particular, the evolution of the critical surface of sidebranching with the control parameters provides a definite test for further investigation of the relevance of sidebranching theories.

In this experiment, two sidebranching modes showing a somewhat large spatiotemporal coherence have been differentiated according to their growth direction. They proved to refer to the same physics. Attention has further been focused on the very occurrence of sidebranching on spatially ordered cellular fronts rather than on its nonlinear regime. Owing to the sensitivity of sidebranching to cell forms, this has required making the cell spacing Λ an effective control parameter by improving the reduction of the usual spatial dispersion of cellular fronts. The sidebranching transition has then been identified by the vanishing of an order parameter and its location has been accurately determined in the parameter space (V,Λ,G) of the system. Its evolution with the control parameters reveals interesting features, especially an apparently paradoxical destabilizing effect of the thermal gradient. This might yield some improvements of the selection of a relevant theory for sidebranching.

The paper is organized as follows. The experimental setup and procedure are reported in Sec. II. Sections III and IV are devoted to a qualitative and a quantitative analysis of the sidebranching transition. A discussion of the results and an analysis of their compatibility with linear convective instability of the cell tip are given in Sec. V. They are followed by a conclusion on this work.

II. EXPERIMENTAL SETUP AND PROCEDURE

The experimental setup aims at pulling a melt into a temperature gradient so as to force it to solidify at a given velocity V. Below we report its configuration, its accuracy, and the procedure required for addressing the sidebranching transition.

A. Configuration

The experimental setup, sketched in Fig. 2, is derived from that initially introduced by Hunt, Jackson, and Brown [37]. It aims at producing a constant and uniform thermal gradient along which samples of alloy are pushed mechanically at a constant speed. We have designed it so as to obtain a large accuracy of the control parameters.

The thermal gradient is produced by two heating (100 °C) and cooling (10 °C) zones separated by a gap of 0.5–2 cm. Sample translation across the thermal gradient is provided by a micro-stepper motor supplemented with a linear ball-screw drive. Observation of the growth front is achieved through an exploded optical stage.

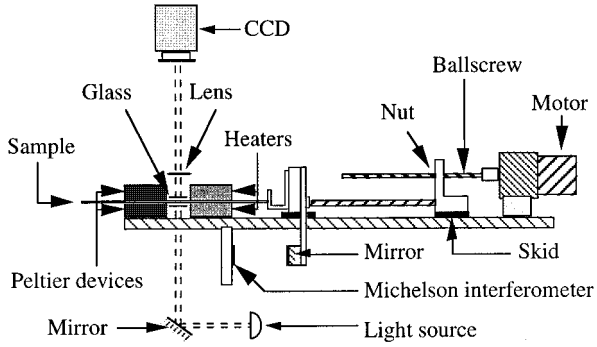

FIG. 2. Sketch of the experimental setup. The relative dimensions have been changed for convenience.

Samples are made of two glass plates, 0.6 mm thick, sandwiching two bands of calibrated Mylar sheets placed on their longer sides and glued with araldite. They thus provide a Hele-Shaw cell $45\times 100\ \mathrm{mm}^2$ large and 50–150 μm thick, depending on the Mylar sheet. They were filled by capillarity with impure succinonitrile purchased from Sigma Chemical Co., St Louis.

A NMR study reveals that the dominant impurity involves an ethylenic chemical bond. As ethylene is used in an intermediate phase of the chemical synthesis of succinonitrile, it is thus presumably the dominant impurity of the mixture. Partition coefficient k of the mixture has been deduced from the melting point of pure succinonitrile ($T_0=58.1$ K [5]) and from the interface temperatures of a planar front solidifying ($T=T_0+mc_\infty/k$) and melting ($T=T_0+mc_\infty$), where c_∞ is the solutal concentration and m the liquidus slope. Meanwhile, the value of mc_∞ has also been obtained. The solutal diffusivity in the liquid phase, D, has been deduced from two different methods: first from the relaxation time, D/kV^2, of a solidifying planar front to equilibrium and, second, from the critical velocity, $V_c\approx DGk/mc_\infty(1-k)$, of the primary instability. Both methods yield the same value of D within experimental accuracy. We obtained $mc_\infty=2\pm 0.2$ K, $k=0.3\pm 0.05$, and $D\approx 1\times 10^{-5}\ \mathrm{cm}^2\ \mathrm{s}^{-1}$.

In both the cooling and heating zones, samples are sandwiched by temperature-controlled surfaces in close contact with them, on both their top and bottom surfaces. Heaters are made of a copper block, 1 cm thick, and a radiator, with a resistance sheet in between. Coolers consist of a stainless block, 0.5 cm thick and a water circulation stage, with a Peltier device in between. The block surfaces, $5\times 5\ \mathrm{cm}^2$, provide the temperature controlled boundaries. Their temperatures are measured by a thermocouple and electronically regulated individually according to a self-tuning algorithm. The gap between coolers and heaters is defined by calibrated spacers.

Preserving close contact, all along sample translation, between large sandwiching thermal surfaces and thin but long samples of different depths raises some practical difficulties. All misalignment must be prevented, while some mechanical degree of freedom is nevertheless necessary so as to fit variable sample depths. In order to avoid delicate mechanical controls and better ensure a permanent contact between the temperature-regulated surfaces and the samples, we have opted for a self-adjusting mechanical setup. First, the top blocks are mechanically fixed so as to ensure the parallelism of their surfaces; thermal dilatation of the heaters is anticipated. Then the bottom blocks are placed on three little springs pushing them upwards so as to keep the samples compressed onto the fixed upper block surfaces.

Sample translation is provided by a linear ball-screw driven stage. The rotation of a ball screw by a stepper motor induces a nut translation, which is transferred to the samples by a pushing stage. Both the pushing stage and the nut are fixed on skids mounted on ball bearings and sliding on a linear track. The screw has a 5-mm pitch. Linking it rigidly to the motor axis proved to reduce vibrations efficiently. The motor is fixed on micropositioners in order to align the screw on the track accurately. It involves 200 steps per revolution and 32 microsteps per step. To minimize the vibration level, it is slowed by Foucault current at the end of each microstep.

Crystalline interfaces were observed according to the usual method based on the evidence of optical aberration induced on an incident parallel light beam by refraction at the growth front. However, in order to minimize growth perturbations, an exploded optical setup has been used instead of a classic microscope so as to decouple the optical stage from the growth setup. It basically consists in a small focal lens yielding large frontal distances and magnifications from 2 to 40. For the sake of a better comparison between growth fronts, the figures of cell patterns presented hereafter will involve the same width of 1040 μm, however. Images were recorded via a charge-coupled device (CCD) camera on a time-lapse video recorder and further analyzed by image processing.

B. Accuracy

Owing to the large size of the samples, care has been taken to avoid buckling of the glass plates so as to ensure good homogeneity of depth. A large Mylar sheet, of the same thickness as the spacer strips, has thus been inserted between the two glass plates prior to gluing. With this, the glass plates could be glued under pressure on their two widest sides so as to ensure the required depth. Relative depth accuracy was better than 5% and remained so after removal of the large Mylar sheet from one of the shortest sample sides.

In order to improve uniformity of the thermal gradient and reduce its fluctuations, the following precautions were taken (Fig. 2). The width of the samples (50 mm) was chosen large with respect to the gap g between the thermal devices (less than 20 mm) so as to suppress end effects on a large part, at least 25 mm, of the front. In addition, the extent of the contact between the thermal blocks and the lateral sides of the setup within which they were inserted was reduced so as to minimize lateral thermal losses. Also, these lateral sides were thermalized by water circulation so as to cut the remaining lateral heat fluxes. On the other hand, in order to reduce radiative and convective perturbations, the thermal blocks were recovered with a reflecting sheet and two horizontal glass plates filling the gap were placed at a small distance above and below the samples. Finally, sufficiently large metallic blocks were used in each thermal device so as to filter external perturbations and reduce their effect on the temperature field of the samples.

Altogether, the above precautions ensure temperature fluctuations on the interface of the order of that measured on the thermal probes, i.e., better than 10^{-1} K. This was checked directly on thermocouples placed inside samples. Finally, direct observation has confirmed the absence of measurable inclinations or distortions, either time dependent or permanent, on steady interfaces.

The transport of the thermal field occurs not only by conduction but also by advection, owing to sample translation. This induces a nonlinear displacement of the isotherms towards the cold boundary and thus a nonuniform thermal gradient. Since these effects grow with pulling velocity, they result in increased drifts of both the melting isotherm and thermal gradient G on the interface. However, the isotherm shifts δz vary on a scale equal to gap g and display, in the range of parameters used here, a relative amplitude $|\delta z|/g$ less than 5%. The relative variation of the thermal gradient on a diffusion length in the vicinity of the interface is then, in any case, less than 2%. In addition, we note that, by symmetry, the shift of the thermal gradient actually vanishes in close vicinity to the middle of the gap. Although the isotherm shift is maximal at this location, we chose to locate the melting isotherm there, so as to minimize the difference between the local gradient on the interface and that expected from a conductive profile. Anyhow, the actual temperature gradient at the interface $G(V,g)$ was calculated with a one-dimensional model of diffusion advection, the effective thermal diffusivity of the sample being deduced from measurements of the temperature field at different V and g.

The regularity of the sample translation was controlled by interferometry. For this, a mirror fixed on the stage pushing the samples was used as the end of an arm of a Michelson interferometer. Measurement accuracy was typically 2.5×10^{-2} μm, allowing a detailed analysis of the sample translation and a control of its perturbations. Two kinds of irregularity have been noticed: one, at large frequencies, consists in vibrations either of the setup or of the interferometer arm; the other, at low frequencies, consists in weak nonlinearities of the translation.

Vibrations are generated by translation. Their amplitude is, *a priori*, given by the microsteps (0.78 μm) but is expected to be smaller, around 0.3 μm, owing to damping by Foucault currents. Their measured amplitudes are ± 0.2 μm at rest, ± 0.4 μm at 1 μm/s, and ± 1.4 μm at 25 μm/s. The increase of vibration amplitudes with translation velocity results from the growth of mirror vibrations as its resonance frequency is approached and thus does not refer to vibration of the sample. Anyway, the vibration time scale (10^{-2} s) is presumably too small compared to those of crystal growth (1 s at least) for inducing noticeable effects.

On the other hand, the weak nonlinearities of the linear drive occurred periodically at each screw turn, i.e., on time scales sufficiently large that they may be felt by the growing interface: 1000 s at a translation speed of 5 μm/s to 150 s at 30 μm/s. They were minimized by accurately aligning the screw on the track and then yielded quasisinusoïdal modulations. The relative amplitude of velocity variation $\delta v/v$ was at most $\pm 3\%$.

C. Experimental procedure

Impure succinonitrile was introduced by capillarity before sample airtightness was achieved by further gluing. Sufficient time was taken for obtaining a noticeable formation of bubbles by demixing. These were then collected at one end of the sample so as to avoid further interface perturbations during solidification. As expected, bubble formation during interface growth then occurred only exceptionally.

Owing to the uncertainty in the composition of the alloy, the critical velocity was systematically measured by imposing a linear ramp of velocity and seeking the occurrence of planar instability. In order to approach the steadiness of the concentration profile, the ramp amplitude was as slow as 0.5 μm/s per hour yielding, for typical critical velocities of 1.5 μm/s, 3 h of growth before instability. Owing to the low pulling velocity (≈ 1 μm/s), this procedure was analogous to a zone melting and resulted in the formation of an inhomogeneous concentration field. It thus required rehomogenizing the mixture before proceeding with further study. This was achieved by diffusion in the liquid phase enhanced by shock-induced advection in order to minimize the homogenization time. Because further studies of interface growth were performed at larger velocities (≈ 10 μm/s), they produced much weaker inhomogeneities and thus fortunately did not require homogenization until after at least five runs.

Without special care, the coherence length of crystal orientation is small, roughly a few cells. Since crystal anisotropy monitors the growth direction of cells or of sidebranches, this may result in pattern spatial disorder, in various dendritic shapes [12,39] or in growth frustration as in the ''algae'' regime [38]. In such cases, accurate analyses of sidebranching features would be compromised and information about growth would mainly be statistical. In order to perform a careful study of the sidebranching transition and a detailed comparison between different runs, we prepared the samples by grain selection in a definite anisotropy state, the directions [100] and [010] being parallel to the sample thickness and the pulling direction. The coherence length of crystalline anisotropy extended up to 100 cells and its fluctuations were minimized to roughly 2 degrees only.

The homogeneity of crystalline anisotropy favored the achievement of well ordered states: the absence of grain boundaries prevented localized phase disturbances and grain drifts along the front; phase diffusion could then proceed over long distances and over long periods to efficiently remove cell spacing gradients. Typical cell spacing dispersions as low as $\delta\Lambda = \pm 5$ μm over 30 cells were achieved in practice (Fig. 3).

The value of cell spacings could be changed by the history of the velocity increase from the onset: usually, a slow continuous ramp favored wide spacing and a quick one small spacing but combinations of increasing and decreasing ramps could yield a large variety of spacings. The range of cell spacing was increased by the fact that, in the same pattern and for the same history, its values slightly differed from grain to grain. We finally notice that, once established, cell spacing evolved very weakly with pulling velocity. The typical range of available cell spacing $\Delta\Lambda$ was about $\Delta\Lambda = 60$ μm at any velocity and any gradients for a typical medium spacing value of 100 μm. We emphasize that each spacing value corresponds not to an average value but to a *definite* value displayed over a large set of cells (Fig. 3). Thus, although spacings were not monitored directly, they

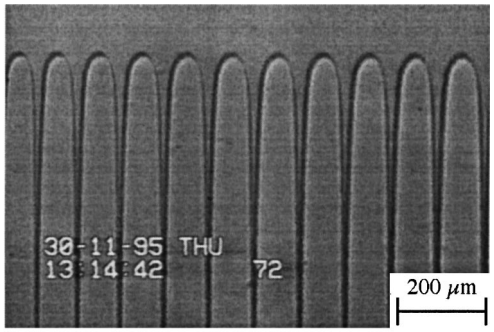

(a)

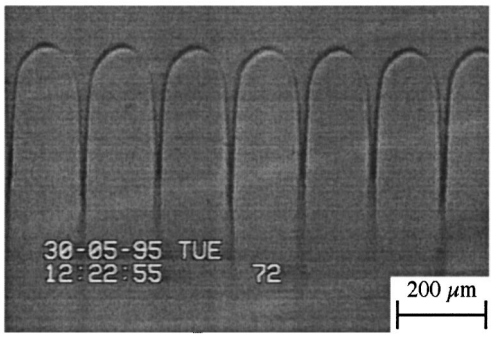

(b)

FIG. 3. Equally spaced cells. Their different spacings illustrate the spacing range involved in the study. (a) $G=140$ K/cm, $V=12$ μm/s, $V_c=2.7$ μm/s, $\Lambda=100$ μm. (b) $G=36$ K/cm, $V=8$ μm/s, $V_c=0.69$ μm/s, $\Lambda=150$ μm.

may nevertheless be considered as an accurate control parameter for the study.

Whatever the pulling velocity considered, each observation began after transient decay. The concentration profile required at least a time of D/kV^2 to achieve equilibrium (about 100 s at 10 μm/s to 3 h at 1 μm/s). The steadiness of the cell pattern was favored by the homogeneity of the crystalline orientation and was achieved within a few diffusion times D/V^2. On the other hand, only crystal growth near the middle of the sample and over one-fourth of its extent has been studied in order to avoid end effects.

In Table I, we report the typical ranges of variables and control parameters involved in the present study.

III. SIDEBRANCHING TRANSITION: QUALITATIVE ANALYSIS

From now on, we restrict our attention to single crystals oriented so that their principal axes are directed along the pulling direction, the sample depth, and the mean front direction. The sidebranching phenomenon consists in the repetitive emission of front distortions by the cell tip and their advection towards the grooves (Fig. 1). We report below its qualitative features.

A. Anisotropy and sidebranching modes

Owing to crystalline anisotropy, sidebranches are expected to grow along the principal crystalline directions $\langle 100\rangle$. Two different kinds of sidebranching modes were observed. The first, shown in Fig. 4(a), is similar to that usually described in the literature. It is characterized by the growth of distortion oriented *within* the sample plane. The other, shown in Fig. 4(b), is similar to the first but displays a different orientation, with deformation taking place along the *perpendicular* direction of the sample depth. It is reminiscent of the 3D oscillation reported by Heslot and Libchaber [12]. In reference to the orientation of these sidebranching modes with respect to the sample plane, we shall call the first mode the parallel mode and the second mode the perpendicular mode.

Both modes were observed either independently [Figs. 4(a) and 4(b)] or together [Fig. 4(c)] depending on pulling velocity V, thermal gradient G, sample depth d, and cell spacing Λ. In particular, the simultaneous occurrence of these modes of distortion gave rise to a 3D dendritic morphology [Fig. 4(c)], largely encountered in the literature. We emphasize here, however, that 3D dendritic distortions actually correspond to the coexistence of *two* perpendicular 2D distortions which can be studied *separately*.

The fact that each mode could be observed alone shows that, in contrast with a previous analysis [12], none of them, especially the perpendicular mode, can be considered as a precursor of the other. On the other hand, at low sidebranching amplitude at least, both actually behave independently of each other, regarding not only their domain of existence but also their amplitude, frequency, and phase. In particular, triggering a mode by a velocity increase did not apparently modify any of the dynamic features of the other mode, so that their coupling, if any, is weak. Owing to this important property, we could hereafter restrict the description to a single mode without losing essential information.

B. Tip steadiness; sidebranch coherence

Cell tips were observed at a large optical resolution of 2 μm. No tip oscillations were noticeable at this accuracy, even at the largest pulling velocities ($V=30$ μm/s). By comparison, the sidebranch wavelengths and amplitudes extended to 40 and 25 μm, respectively, i.e., a larger order of magnitude. Similar conclusions of tip steadiness have been drawn in free growth [5–9].

Observations of sidebranches over many periods revealed a noticeable coherence of sidebranching emissions, from both a spatial and a temporal viewpoint. Determining a rel-

TABLE I. Typical ranges of variables and control parameters used in this work.

Parameter	g (mm)	G (K/cm)	V_c (μm/s)	V (μm/s)	V/V_c	d (μm)	Λ (μm)	Pe
Minimum	5	36	0.7	6	2.8	50	50	0.5
Maximum	20	140	3	50	37	150	250	4.5

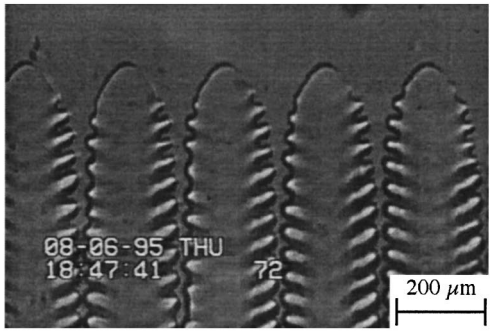

(a)

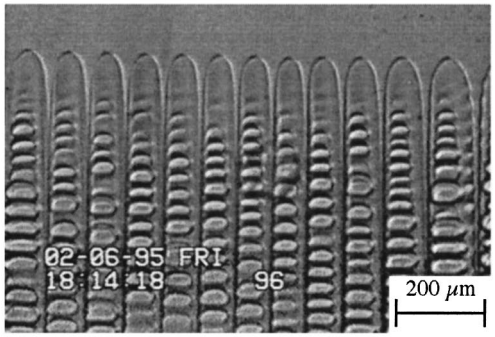

(b)

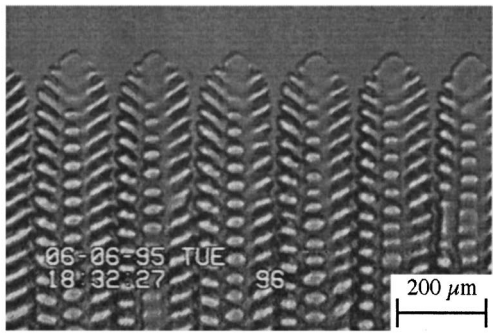

(c)

FIG. 4. Equally spaced cells showing the sidebranching modes: (a) parallel mode ($G=50$ K/cm, $V=10$ μm/s, $V_c=0.8$ μm/s, $\Lambda=230$ μm); (b) perpendicular mode ($G=79$ K/cm, $V=18$ μm/s, $V_c=1.44$ μm/s, $e=122$ μm); (c) combination of the parallel and perpendicular modes ($G=51$ K/cm, $V=18$ μm/s, $V_c=0.93$ μm/s, $\Lambda=180$ μm, $e=122$ μm).

evant measure of the level of coherence requires a statistical analysis that goes beyond the scope of this paper. Nevertheless, Figs. 4(a)–4(c), show a phase order extending over more than five cells, i.e., over a distance significantly larger than the diffusion length. Also, direct observations show a phase coherence of sidebranching emissions extending over roughly ten periods, i.e., over a time much larger than the coherence time of any fluctuation, especially thermodynamic fluctuations, in the system.

C. Order parameter

At the optical resolution involved in our experiment, both sidebranching modes display a definite velocity onset separating stable and unstable domains. In its vicinity, sidebranching begins to be observed [Figs. 5(a) and 5(b)]. Although this onset regime is qualitatively similar for both

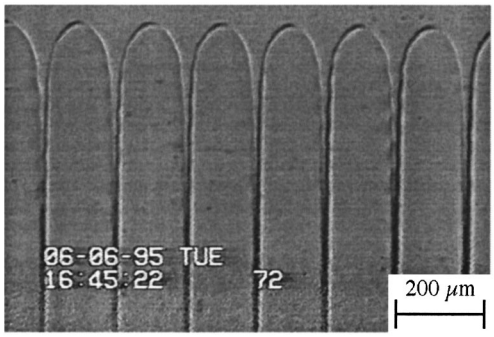

(a)

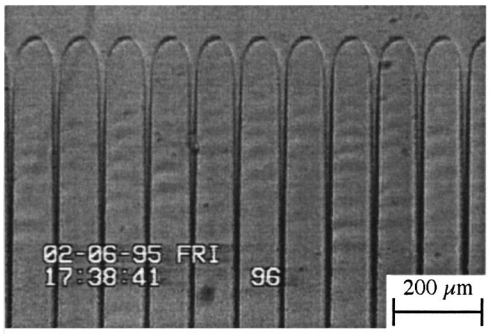

(b)

FIG. 5. Onset of sidebranching on equally spaced cells: (a) parallel mode ($G=50$ K/cm, $V=10$ μm/s, $V_c=0.92$ μm/s, $\Lambda=160$ μm); (b) perpendicular mode ($G=78$ K/cm, $V=12$ μm/s, $V_c=1.43$ μm/s, $e=122$ μm).

modes, it is, however, much more accurately identified for the parallel mode than for the perpendicular mode since the sidebranch modulations are transverse to the light beam in the former case [Fig. 5(a)] whereas they are parallel to it in the latter case [Fig. 5(b)]. For this reason, we shall focus attention on the parallel mode in the following, although a similar analysis would also hold for the perpendicular mode.

At transition to sidebranching, the cellular forms show dynamic wavy modulations which stand as elementary sidebranches. A typical digitalized profile of a cell boundary above this critical state is presented in Fig. 6. It shows distortion of the mean profile whose amplitude grows with the

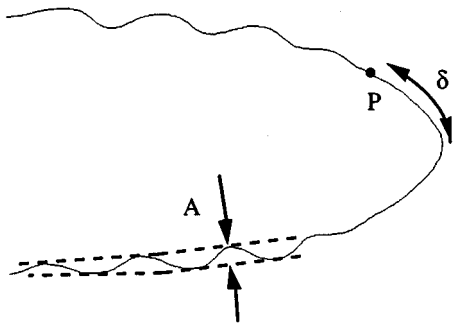

FIG. 6. Skeleton of a cell emitting sidebranches: $V=20$ μm/s, $\Lambda=150$ μm, $G=78$ K/cm. Point P refers to the first noticeable sidebranch, δ to its distance from the tip, and A to sidebranch amplitude.

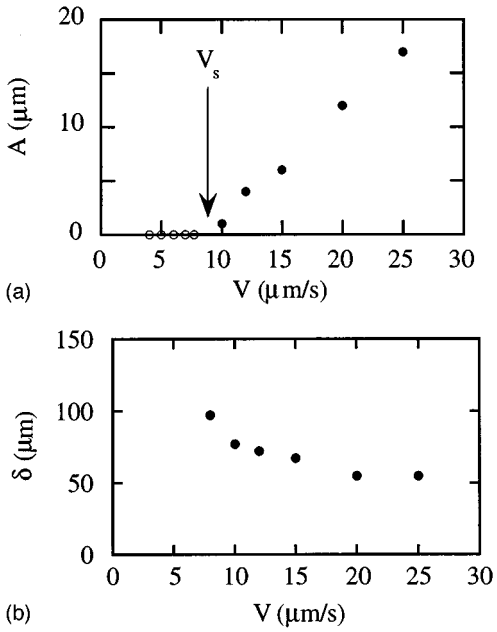

FIG. 7. Evolution at fixed Λ and increasing V of (a) sidebranching amplitude A: open circles refer to zero amplitude and $V_s = 7.9\ \mu$m/s to the onset of sidebranching; (b) distance δ of the first visible sidebranch from the tip.

distance from the tip, then saturates and eventually shrinks in the grooves. Some time later, the whole distortion would have been advected along the front, but additional elementary sidebranches would have arisen near the tip. Furthermore, all the interface distortions seem to emerge from the same specific location P where modulation of the mean profile first begins to be visible.

Two quantities worth measuring: the distance δ of the first noticeable sidebranch P from the tip and a characteristic distortion amplitude A (Fig. 6). The value of δ has been determined from a series of profiles taken over several sidebranching periods. Considering the sidebranching amplitude at a given point of the front would rely on a somewhat arbitrary location since its value varies with the distance from the tip. To get a more intrinsic characterization of the sidebranching phenomenon, we therefore define A as the maximum sidebranching amplitude over the cell profile and over time. This provides us with a global variable characteristic of the cell state only.

At *fixed* thermal gradient G, cell spacing Λ, and optical resolution, the typical evolution of δ and A with velocity are shown in Figs. 7(a) and 7(b). We note that, at our accuracy, A vanishes below some onset of velocity V_s. Conversely, δ displays no peculiar value, even at high velocities, and no specific evolution, even in the vicinity of V_s. In contrast with δ, sidebranching amplitude A thus provides an objective definition of the onset of sidebranching in the system: cells emit no sidebranching in the $A=0$ domain, infinitesimal ones at the onset $A=0^+$, and noticeable ones in the $A>0$ domain. In the following, we shall use this criterion $A=0^+$ to determine the critical surface separating the stable cell domain $A=0$ from the ''dendritic'' cell domain $A>0$ in the control parameter space.

Depending on the nature of the sidebranching mechanism, noise amplification or oscillation, the vanishing of A may or may not depend on optical resolution. In the former case, the onset of sidebranching would only be apparent; in the second case, it would be real. The determination of its nature would require a large variation of the optical resolution, which goes beyond the scope of the present study. Nevertheless, we stress that, at the *fixed* optical resolution used here, the vanishing of A provides, in either of the above cases, a definite characterization of sidebranching liable to improve understanding of it.

D. Dependence on cell spacing, sample depth, and velocity

We address the qualitative dependence of the sidebranching transition on cell spacing, sample depth, and pulling velocity. Patterns displaying either a single cell spacing or a spacing gradient were studied. Also, not only samples involving uniform depth but also those displaying a wedge parallel to the mean front direction were considered.

In any case, increasing solely the velocity at otherwise fixed parameters enhanced sidebranching of both the parallel and the perpendicular modes. This result confirms the well-known role of velocity regarding sidebranching and shows its relevance to either of the two sidebranching modes and either to equally or differently spaced patterns.

In this paragraph, we now restrict our attention to the parallel mode. On patterns involving single cell spacing and uniform sample depth, this mode occurs on all cells [Figs. 4(a), 4(c), 5(a)] or none [Figs. 3(a), 3(b), 4(b), and 5(b)] depending on velocity and cell spacing. On patterns involving a spacing range and a uniform sample depth, one notices coexistence between stable and unstable cells separated by half-unstable cells, i.e., cells unstable on a single side only as stressed in Ref. [2] [Fig. 8(a)]. In agreement with the moderate value of the Péclet number, cell stability thus appears influenced by the nearest neighboring cells only, so that a stability analysis with respect to individual spacing may be relevant, although less accurate than in equally spaced cells: only cells involving spacing wider than a definite value then show sidebranching with a mean frequency function of the pulling velocity but independent of cell spacing and sample depth [Fig. 8(a)]. Finally, in samples involving a depth gradient along the front, no difference regarding parallel mode was observed. Following these observations, the parallel mode therefore stands not as a collective mode, but as a cellular mode whose onset depends on both spacing and velocity but not on sample depth.

The observations made on the perpendicular mode were fairly similar. In patterns involving single cell spacing and uniform depth, it occurred on all cells [Figs. 4(b), 4(c), and 5(b)] or none [Figs. 3(a), 3(b), 4(a), and 5(a)] depending on the velocity. In patterns involving a cell spacing range and uniform sample depth, it still appeared on the whole front [Figs. 8(b), 8(c)] or not [Fig. 8(a)], but showed the same onset and the same mean frequency irrespective of cell spacing [Figs. 8(b), 8(c)]. Finally, in samples involving a depth gradient along the front direction, the perpendicular mode only appeared above a threshold of sample depth (Fig. 9); its mean frequency, however, appeared independent of both cell spacing and sample depth. According to these observations, the perpendicular mode stands as a cellular mode whose on-

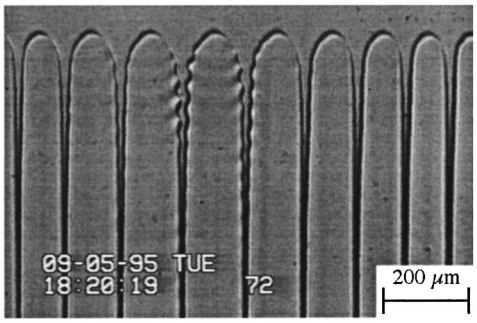

(a)

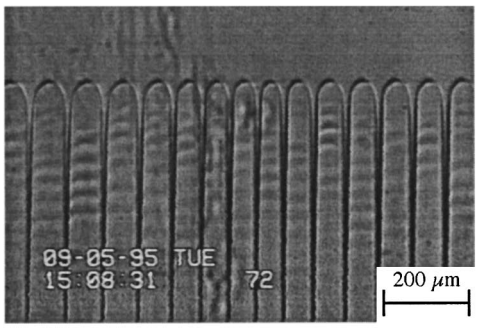

(b)

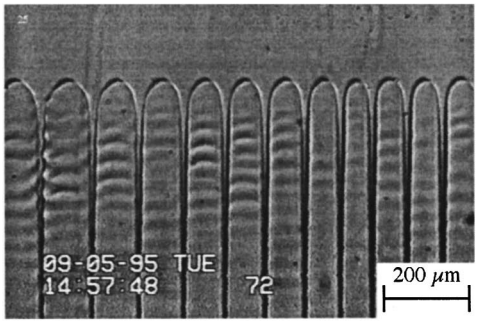

(c)

FIG. 8. Differently spaced cells showing the sidebranching modes: (a) parallel mode arising on one cell and its half-neighbors ($G=51$ K/cm, $V=19$ μm/s, $V_c=0.98$ μm/s); (b) perpendicular mode arising on all cells independently of their spacing ($G=80$ K/cm, $V=30$ μm/s, $V_c=1.53$ μm/s, $e=108$ μm); (c) combination of the parallel and perpendicular modes ($G=79$ K/cm, $V=24$ μm/s, $V_c=1.51$ μm/s, $e=108$ μm).

set depends on both sample depth and pulling velocity but not on cell spacing.

When observed together at a fixed thermal gradient, the two modes showed the same mean frequency, which was dependent on the pulling velocity alone [Figs. 4(c), 8(c)]. As no frequency locking was noticed at the occurrence of a second mode, this observation means that mean sidebranching frequency is independent of cell spacing and of sample depth, in agreement with the conclusions separately drawn for each mode.

The behaviors of the parallel and the perpendicular modes thus show a large similarity. Apart from pulling velocity, their onset depends on a single geometrical size related to their sidebranching direction: cell spacing for the parallel mode and sample depth for the perpendicular mode. Since, from a more general viewpoint, they behave independently

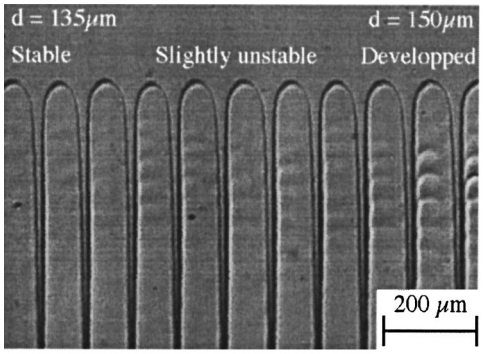

FIG. 9. Localization of the sidebranching transition in perpendicular mode by depth gradient. The small difference of depth from left to right is sufficient to go from a stable to a developed sidebranching regime.

of one another, each refers to growth within a definite plane with no dependence on the conditions prevailing on the remaining direction. They therefore stand as a two-dimensional growth phenomenon.

E. Marginal stability; critical surface

The experimental originality of our study was to significantly reduce the scattering of both crystal orientation and cell spacing over the growth front. This allowed us to observe two well-defined transitions from steady cells to cells emitting sidebranching, one referring to the parallel mode and the other to the perpendicular mode. As mode coupling is negligible, the concept of sidebranching transition, which has been questioned following the scattering induced by spatial disorder [2,13], is actually validated here for each mode. It is supported, for the parallel mode, by the identification of an order parameter, the sidebranching amplitude A, as defined in Sec. III C.

Beyond the concept of transition, sidebranching appears here as a cellular instability involving a stable domain for $A=0$ and an unstable domain for $A>0$. This, *a priori*, does not exclude any origin, intrinsic or extrinsic, for sidebranching. On the other hand, the fact that, at the accuracy of our observations, we noticed no jump of order parameter A at the transition to sidebranching, suggests that the sidebranching instability is supercritical. This is corroborated by the absence of any hysteretic behavior regarding sidebranching.

The above analyses show that, for the parallel (perpendicular) mode, the critical surface S defined by $A=0^+$ depends on pulling velocity V, cell spacing Λ (sample depth d), thermal gradient G, and mixture composition, but not on the history or the stability of the alternate mode. As the mixture composition kept constant throughout the study, we shall therefore parametrize S by V, Λ (d) and G: $S\equiv S(V,\Lambda,G)$. This provides critical functions $V_s(\Lambda,G),\Lambda_s(V,G)$ $[V_s(d,G),d_s(V,G)]$, which correspond to the onset of velocity V_s and the onset of spacing Λ_s (d_s) for sidebranching: $A>0$ for either $V>V_s$ or $\Lambda>\Lambda_s$ ($d>d_s$); $A=0$ for either $V<V_s$ or $\Lambda<\Lambda_s$ ($d<d_s$). The following section is devoted to quantitatively determining V_s, Λ_s, and the critical surface S.

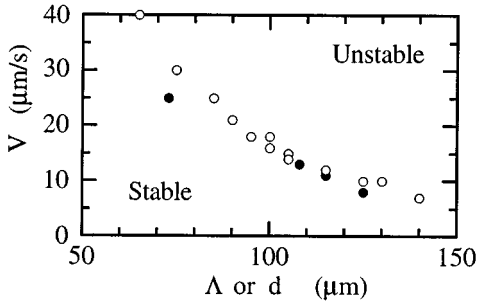

FIG. 10. Onset of sidebranching for parallel mode $V_{s\parallel}(\Lambda)$ (open circles) and for perpendicular mode $V_{s\perp}(d)$ (full circles) at $G=110$ K/cm as a function of either spacing Λ or sample depth d, respectively. The collapse of data shows similarity.

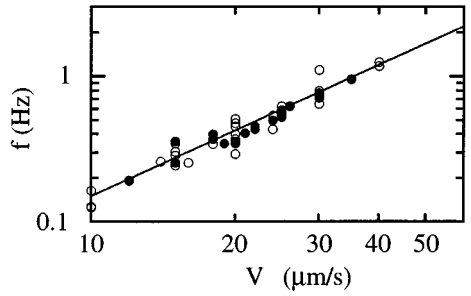

FIG. 11. Mean frequency over a few cycles as a function of velocity. The line of slope 3/2 shows the relevance of mean scaling law $f^2 \alpha V^3$. Open symbols refer to the parallel mode and full symbols to the perpendicular mode.

IV. SIDEBRANCHING TRANSITION: QUANTITATIVE ANALYSIS

After having addressed the physical equivalence of the two sidebranching modes, we perform a systematic study of their sidebranching transition. This allows us to analyze the role of the different control parameters and achieve the determination of the critical surface for sidebranching.

A. Physical equivalence of the sidebranching modes

The qualitative similarity of the sidebranching modes suggests their physical equivalence. To test this property, we compare below at fixed thermal gradients the quantitative evolution of onset V_s and frequency f of sidebranching displayed by the two modes. As each mode showed no dependence on the spacing relative to the other mode, the functions to be compared involve, at each gradient, a single spacing variable: Λ for the parallel mode and d for the perpendicular mode. Those relative to the parallel (perpendicular) mode will be indexed by $\parallel$ ($\perp$).

1. Similarity of onset evolutions

We compare the onset evolutions $V_{s\parallel}(\Lambda,G)$ $[V_{s\perp}(d,G)]$ of the parallel [perpendicular] mode with spacings Λ (d). Figure 10 displays, on the same graph, the marginal stability curves obtained at a given gradient $G=110$ K cm^{-1} and at a fixed mixture composition. A collapse of the two curves $V_{s\parallel}(\Lambda)$ and $V_{s\perp}(d)$ is observed. This confirms that the onset of each mode is only dependent of its own spacing parameter and shows that the relationship between spacing and onset is the same for the two modes: $V_{s\parallel}(\cdot)=V_{s\perp}(\cdot)$.

2. Similarity of frequency evolutions

Extension of the comparison between the modes to the instability domain can be performed by addressing either sidebranching amplitudes or sidebranching frequencies. As measuring sidebranching amplitudes on the same grounds for both modes is problematic, we restrict the analysis to sidebranching frequencies f.

Figure 11 shows sidebranching frequencies $f_{\parallel}(V), f_{\perp}(V)$ of the two modes as a function of velocity V. Scattering is noticeable on each curve. It stems from the weak coherence time of sidebranching, according to which frequencies can only be measured on few periods. The collapse of these curves is nevertheless noticeable at the accuracy of our measurements. It first means that sidebranching frequencies are much less dependent on cell spacing Λ and sample depth d than on pulling velocity V. It then shows that the dependence of frequency on velocity is the same for the two modes: $f_{\parallel}(\bullet)=f_{\perp}(\bullet)$. This corroborates the qualitative observations of the same frequency for both modes at a given velocity and gradient, even for differently spaced cells and for different sample depths.

The mean frequency increases with pulling velocity V according to a power law $V^3=\mu f^2$, where μ is a constant of about 5×10^4 μm^3 s^{-1} (Fig. 11). This corresponds to sidebranch wavelengths $\lambda_{sb}=V/f$ scaling as $\lambda_{sb}^2 V=\mu$, in agreement with [11,2].

3. Physical equivalence

The above similarities show that the two modes behave in the same way regarding their onset and their frequency. Despite the differences pertaining to their boundary conditions, they thus presumably refer to the same physics. We postpone to Sec. V A the discussion of this physical equivalence.

B. Transition curves

Beyond the above physical equivalence, the parallel mode appears much easier to study in practice than the perpendicular mode. This stems from its better visibility and from the fact that it allows a continuous scan of cell spacing, whereas in samples involving a uniform depth, a single spacing value is available for the perpendicular mode. To determine sidebranching transition curves accurately, we shall therefore mainly focus our attention on the parallel mode in the following.

Since the Péclet number is about unity, cells are at least coupled to their nearest neighbors. Therefore, the onset of their parallel mode might not be relevant to their spacing if they are surrounded by cells involving different spacing. To avoid this, we shall hereafter restrict the analysis to patterns displaying equally spaced cells. Although this situation refers, strictly speaking, to an assembly of cells, the cellular rather than collective nature of sidebranching modes and their physical equivalence ensures that, regarding the onset of sidebranching, it also pertains to the behavior of a single cell in a channel.

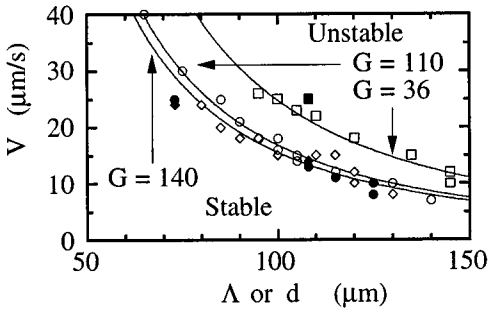

FIG. 12. Onset of sidebranching for the parallel mode $V_{s\parallel}(\Lambda)$ (open symbols) and the perpendicular mode $V_{s\perp}(d)$ (full symbols) at various gradients as a function of either spacing Λ or sample depth d, respectively. Squares: $G=36$ K/cm; circles: $G=110$ K/cm; diamonds: $G=140$ K/cm.

Figure 12 shows, for different thermal gradients G, the onset of velocity $V_{s\parallel}$ of the parallel mode as a function of cell spacing Λ: $V_{s\parallel}(\Lambda,G)$. A few additional points referring to the onset of velocity $V_{s\perp}(d,G)$ of the perpendicular mode as a function of sample depth d are included for thoroughness.

Above each curve stands the unstable domain regarding sidebranching. Increasing V at constant spacing Λ and gradient G thus yields sidebranching: one recovers the well-known destabilizing effect of the pulling velocity regarding sidebranching [2,3]. Also, increasing the cell spacing Λ at fixed velocity V and gradient G leads from the stable to the unstable regime: cell spacing is destabilizing with respect to sidebranching. This effect agrees with previous observations [13] and with the destabilizing role of the averaged cell spacing $\langle\Lambda\rangle$ in the vicinity of the cell-dendrite transition [2,10]. It is, however, confirmed here beyond the statistical level for each cell spacing considered separately.

The last effect regarding stability is surprising: increasing thermal gradient G at fixed velocity V and spacing Λ enhances sidebranching. This might appear at first glance somewhat paradoxical since the primary effect of the thermal gradient consists in stabilizing the growth front by narrowing the distance between isothermal lines, as, for instance, in planar instability. We postpone to Sec. V D the discussion of its significance.

C. Critical surface

To better characterize the critical surface on which the onset of sidebranching is observed, we look to identifying it in nondimensional variables. These must be obtained within the variables characterizing the state of the front, V and Λ, and those pertaining to the growth regime, i.e., critical velocity V_c, diffusion length $l_D=D/V$, thermal length $l_T=m\Delta c/G\approx D/V_c$, and capillary length $d_0=\gamma/m\Delta c$. As $l_T/l_D\approx V/V_c$, the diffusion length may be removed from the set of essential variables. The equation of the critical surface may then be sought within the following nondimensional form: $\nu=\psi(\Lambda/d_0,l_T/d_0)$, where ν denotes the reduced velocity V/V_c.

In the present experiment, the cell spacing stands in an intermediate asymptotic limit regarding d_0 and Λ: $d_0\approx 13\times10^{-3}$ μm, $\Lambda\approx$50–100 μm, $l_T\approx500$ μm so that $d_0\ll\Lambda<l_T$. Then, both Λ/d_0 and l_T/d_0 are several orders of magnitude wide so that a self-similar asymptotic regime of the second kind may be assumed [40]. According to this, $\psi(\bullet,\bullet)$ should stand as a power law of its variables:

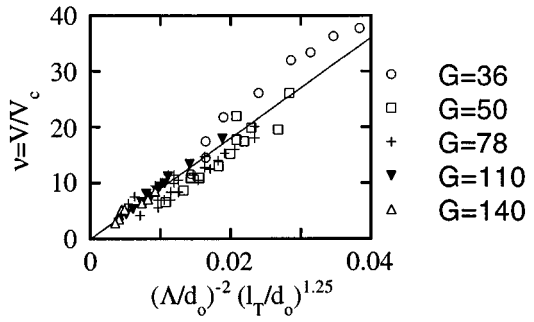

FIG. 13. Collapse of the critical curves on the scaling law (1) and (2) for various $\nu=V/V_c$, Λ, and G (K/cm) and for $d_0=0.013$ μm and $D=1\times10^{-5}$ cm^2/s.

$$\nu=c\left(\frac{\Lambda}{d_0}\right)^{\beta}\left(\frac{l_T}{d_0}\right)^{\gamma}. \tag{1}$$

As γ, $m\Delta c$, and therefore d_0 have been kept constant in the present experiment, we have fitted ν with respect to Λ and l_T. The following values have been selected with a quality factor $R=0.95$:

$$c=900\pm20,\quad \beta=-2\pm0.1,\quad \gamma=1.25\pm0.1. \tag{2}$$

They correspond to

$$V\Lambda^2G^{1/4}=C, \tag{3}$$

where C only depends on k, mc_∞, D, and d_0.

The collapse of the critical curves of Fig. 12 onto a single curve defined by relations (1) and (2) is shown in Fig. 13. According to this, the critical surface is well characterized by scaling laws (1)–(3) in our experiment.

As power laws are weakly sensitive to suitable coupled variations of both prefactors and exponents, this global agreement between data and scaling law cannot be used for an accurate identification of exponents. In particular, as a large family of power laws could equally well fit our data; the uncertainty on each scaling exponent considered separately is somewhat larger than might have been expected on a simple level. Studying the effect of variations of c, β, and γ on the agreement between power law relations and data, we estimate this uncertainty at $\delta\beta=\delta\gamma=\pm0.1$. Despite its high value, we may ensure that, in relation (3), the exponents of Λ and G are certainly positive, in agreement with the destabilizing nature of V, Λ, and, especially, G in this experiment.

V. DISCUSSION

The main features of sidebranching observed in Secs. III and IV refer to the physical equivalence of the two sidebranching modes, to the existence of a critical surface showing a destabilizing effect of the thermal gradient, and to some

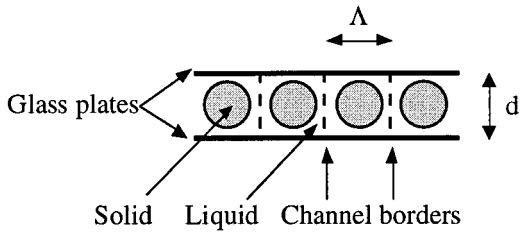

FIG. 14. Sketch of a cut of the sample showing the different boundary conditions applying to parallel and perpendicular modes.

noticeable coherence of sidebranching. We discuss them below, in particular in the light of the noise amplification theory.

A. Sidebranching and boundary conditions

Since both sidebranching modes bear a two-dimensional nature, the boundary conditions relevant to each of them refer to those encountered in their growth plane, i.e., along the sample depth for the perpendicular mode and within the sample plane for the parallel mode (Fig. 14). They thus display the following differences:

The perpendicular mode involves a *fixed* boundary, the glass plates, enclosing a single cell (Fig. 14). It is thus similar to a two-dimensional sidebranching instability of an isolated cell growing in a capillary. On the other hand, the parallel mode involves a *free* boundary, the channel border (Fig. 14), which separates a cell from the remaining pattern. There, neither boundary dynamics nor coupling with neighboring cells can be excluded.

The importance of cell boundary conditions with respect to cell dynamics may be stressed by analogy with another cell instability, vacillating-breathing instability, in which both cell tip and cell width oscillate [36]. If fixed boundaries are imposed, the instability addresses a single cell; it then refers to a 1Λ-O instability, the term O meaning oscillating and the term 1Λ meaning that, in a cellular array, the period of instability is equal to a cell spacing Λ. If free boundaries are allowed, the groove between two cells can now oscillate not only in width but also in position. This may correspond, for instance, to a phase opposition between neighboring cells, according to which the spatial periodicity of the instability extends on two cell spacings. This case is referred to as a 2Λ-O instability. Stability analysis and observations then reveal that this mode is much more dangerous than the former mode [36]: fixed or free boundary conditions are not physically equivalent here.

This example shows that some information regarding sidebranching may actually be gained from the physical equivalence of the sidebranching modes. It implies the irrelevance of both cell coupling and cell boundary dynamics as to sidebranching instability. The former irrelevance means that sidebranching refers not to the pattern mode but to a cell mode. It thus involves unstable wavelengths λ all smaller than cell spacing ($\lambda<\Lambda$) and therefore does not rely on the dangerous wave-number interaction between the primary spacing wave number $2\pi/\Lambda$ and its half [36]. The latter irrelevance implies that the dynamics of the flux lines delimiting a cell domain, and thus the phase difference between the sidebranches of adjacent cells, are not essential with respect to the onset of sidebranching.

Altogether, these conclusions show that sidebranching stands as a single-cell instability involving a two-dimensional nature, negligible coupling with the third dimension, and, regarding its onset, no dependence on the nature of the cell boundaries. In particular, even if cells are immersed in a pattern in the present experiment, their sidebranching instability does not refer to a collective mode but, instead, to the instability of a single cell growing in a channel.

B. Average spacing, single-cell spacing, and sidebranching transition

In the literature, the cell-dendrite transition has been scanned by different means addressing either the mean behavior of cells [2,3,10,11] or their individual behavior [13,41]. In the former case, cell spacing is defined in average over the front and turns out, in practice, to be slaved to velocity and thermal gradient. In the second case, cell spacing is considered as a feature relevant to each cell; it may thus take different values at a given velocity and at a given gradient. The present experiment fits with the latter kind of analysis by considering cell spacing as an independent control parameter of sidebranching instability. The two different ways of considering cell spacing have important consequences on the concept of sidebranching transition.

1. ''Average spacing'' approach

In this approach, cells and dendrites are considered as two different branches of solutions for average spacing: the cell branch and the dendrite branch are hereafter labeled $\langle\Lambda_c\rangle$ and $\langle\Lambda_d\rangle$, respectively. Both are only controlled by the relative velocity v and the thermal gradient G: $\langle\Lambda_c\rangle \equiv\langle\Lambda_c\rangle(v,G)$; $\langle\Lambda_d\rangle\equiv\langle\Lambda_d\rangle(v,G)$ [10]. As seen in [2], this point of view is relevant insofar as one can accommodate large standard deviations of cell spacing. Whereas this is the case from a practical viewpoint, it is not from a fundamental one. In particular, we notice that parametrizing the system states by v and G only winds up removing the cell spacing Λ from the set of control parameters. Then dendrites appear more as another growth state *beside* that referring to cells than as an actual dynamic state of cells. In particular, in this framework, the cell-dendrite transition is referred to as a jump between branches of solutions and not as a transition of a given branch, the cell branch, to a dynamic regime [2,3,10].

At a fixed thermal gradient, the dendrite branch displays a decrease of spacing with velocity whereas the cell branch shows a decrease at high and low velocity with an increase in between (Fig. 15) [10]. The latter behavior yields a so-called S shape of the cell branch, which, at high velocities, merges with the dendrite branch. The cell-dendrite transition is then located in the rising part of the curve [2,10]. This corresponds not to a definite location in the (v,G) plane but to a domain mainly corresponding to the deep-cell regime. At various thermal gradients, the transition appears as the intersection between the cell branch and the dendrite branch. This criterion for sidebranching, i.e., $\langle\Lambda_c\rangle(v_s,G_s) =\langle\Lambda_d\rangle(v_s,G_s)$, yields the following scaling for the critical

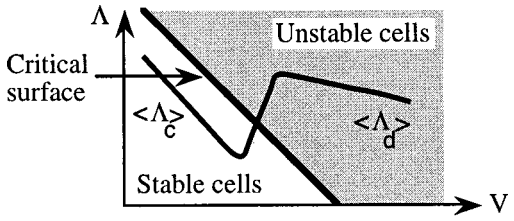

FIG. 15. Comparison between the ''average spacing'' and the ''single-cell spacing,'' approaches. In the ''average spacing'' approach, the growth state is defined by an average spacing value. This yields a cell branch $\langle\Lambda_c\rangle$, a dendrite branch $\langle\Lambda_d\rangle$, and the cell-dendrite transition in between. In the ''single-cell spacing'' approach, a two-dimensional domain is accessible. Inside it, a critical surface separates a stable domain for sidebranching from an unstable one.

surface: $l_D/d_0=(l_T/d_0)^{4/5}$ [15]. It corresponds to $\nu_s=(d_0V_c/D)^{1/5}=\mu G^{0.5}$, where $\mu=mc_\infty(1-k)/kd_0$ is, on each run, a constant. According to this approach, thermal gradient G is thus, on ''average,'' *stabilizing* with respect to sidebranching.

2. ''Single-cell spacing'' approach

By comparison to the ''average spacing'' approach, the approach followed here may be termed a ''single-cell spacing'' approach since the cell spacing is treated not as an average quantity but as a definite one on a given cell. Then the transition is identified by an order parameter, the sidebranching amplitude, and the critical surface $A=0^+$ appears to be parametrized not only by ν and G but also by Λ. As the transition is, at our accuracy, supercritical, it is continuous with respect to A. It then cannot be related to a jump between branches of solution, since this would likely trigger finite amplitude sidebranches and thus a discontinuity of A. Instead, it appears as a dynamic transition of a *single* branch of solution, which, at convenience, may be viewed as triggered by a change of V, G, or Λ. Then thermal gradient G is, on a given cell, *destabilizing* with respect to sidebranching.

3. Link between the two approaches

The ''average spacing'' approach aims at identifying the mean behavior of growth fronts. Here, their statistical state is implicitly described by a probability distribution function (pdf) $p(\Lambda)$ of cell spacing Λ, which, in practice, is governed by V and G: $p(\Lambda)\equiv p(\Lambda;V,G)$. Combined with the results of the ''single-cell spacing'' approach, the ''average spacing'' description may then be understood as a convolution of this pdf with the behavior of individual cells along the front F: the average cell spacing $\langle\Lambda\rangle$ is given by $\langle\Lambda\rangle=\int_F\Lambda p(\Lambda;V,G)d\Lambda$ and the mean dynamic state is linked to the mean value $\langle A\rangle$ of the sidebranching amplitude over the front: $\langle A\rangle=\int_F A(V,\Lambda,G)p(\Lambda;V,G)d\Lambda$. Here, cell spacing Λ no longer stands as a control parameter. In particular, the fact that the average spacing $\langle\Lambda\rangle$ varies with V and G shows that, in practice, the pdf $p(\Lambda;V,G)$ involves large variations with the control parameters. It thus mainly controls the low (large) value of $\langle A\rangle$ and thus the location of the cellular (dendritic) branch.

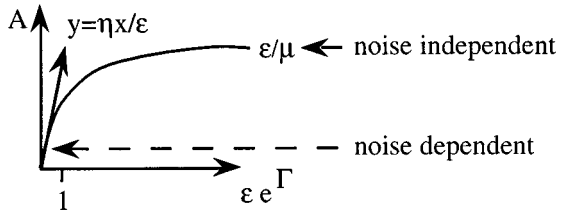

FIG. 16. Crude model of noise (η) amplification (Γ), feedback (ε), and saturation (μ). As the feedback increases, the system turns from a noise-controlled behavior ($A\approx\eta e^{\Gamma}$) to an intrinsic behavior ($A\approx\varepsilon/\mu$).

According to the above analysis, the S shape of the cell-dendrite transition therefore essentially results from the evolution with V and G of the spacing pdf and negligibly on that of sidebranching amplitude $A(V,\Lambda,G)$. Beyond its practical interest, it thus does not refer to fundamental features of the sidebranching phenomenon itself.

C. Local convective instability: The noise amplification theory

The selective amplification of noise has been proposed as a fundamental mechanism for sidebranching. It consists in a convective instability triggered at the tips of growth fronts by the surrounding noise. Here, the instability undergone by tips is similar to the primary instability of a planar front but distortions are advected towards the grooves. Meanwhile, the distortion wavelength increases owing to the stretching induced by tangential flow. It then parametrizes the growth time σ of the distortion amplitude. At a given distance l from the tip measured in terms of curvilinear abscissa s, this results, within a WKB approximation, in a net growth factor $\Gamma(l)$ given by the convolution of growth rates $\sigma(s)$ over the front:

$$\Gamma(l)=\int_{s=0}^{s=l}\frac{\sigma(s)}{v_\tau(s)}\,ds. \tag{4}$$

Here, the origin of curvilinear abscissa, $s=0$, is located at the tip and v_τ stands for the tangential velocity along the front.

Sidebranching amplitude $A(l)$ at a distance l from the tip is given by

$$A(l)=A(0)\exp\Gamma(l), \tag{5}$$

where $A(0)$ stands for the noise amplitude at the tip. Although distortions are already present from the tip, they become visible when the amplitude $A(l)$ crosses an onset value A_c linked to the optical resolution. This provides a criterion for the distance δ of sidebranching birth to the tip: $A(\delta)=A_c$.

The noise amplification theory has received considerable improvements in free growth where wave packets and needle crystals selected by anisotropy of surface tension have been considered [19,20,22,23]. By comparison, only its basic framework has been transposed to directional solidification [30]:

(i) The growth rate σ is given by the dispersion relation of the planar instability, with renormalized normal velocity V and critical velocity V_c to account for the variation of the front normal $\mathbf{z}\rightarrow\mathbf{n}$ and the normal thermal gradient $G \rightarrow G\ \mathbf{z}\cdot\mathbf{n}$: $V\rightarrow V\ \mathbf{z}\cdot\mathbf{n}$, and $V_c\rightarrow V_c\ \mathbf{z}\cdot\mathbf{n}$. Denoting q as the wave number of the perturbation, σ is written as

$$\sigma = q(V-V_c)\mathbf{z}\cdot\mathbf{n} - \frac{V^2|\mathbf{z}\cdot\mathbf{n}|^2}{D} - Dd_0q^3. \tag{6}$$

(ii) The tangential velocity of perturbations along the front originates from two contributions: one, $V\mathbf{z}\cdot\boldsymbol{\tau}$ corresponds to the advection velocity along the tangent vector $\boldsymbol{\tau}$ of a steady form, which advances at velocity $V\mathbf{z}$ in a medium at rest; the other, $-V_c\mathbf{z}\cdot\boldsymbol{\tau}$, describes the migration of perturbations along the front in the direction of the tangential thermal gradient, i.e., towards low concentration regions. Both give

$$v_\tau = (V-V_c)\mathbf{z}\cdot\boldsymbol{\tau}. \tag{7}$$

(iii) The stretch of perturbations may be derived by stressing that, in a steady state of sidebranching, there can be no phase accumulation on any point of the front. Therefore, the phase velocity of perturbations, qv_τ, must be constant along the front: $qv_\tau = \text{const}$.

Since the tangential velocity vanishes at the tip, these determinations yield in relation (4) a singular kernel at $s=0$, which would drive a divergence of the integral. This simply comes from the fact that, in principle, perturbations can grow an infinite amount of time at the tip since they are not advected. This effect can be removed by introducing a cutoff length that specifies the lower limit of the integration domain. Then the tip itself is excluded from the instability domain, but its singular nature in this problem remains: the net growth factor is controlled by the cutoff length.

Taking as the cutoff length the most unstable wavelength λ_s given by the dispersion relation of the planar instability, Sarkar obtained, within a circular approximation of the form of the front near the tip, the following relationship [30]:

$$\Gamma = \frac{2}{3}\frac{2\pi R}{\lambda_s} = \frac{2}{3}\frac{R}{(l_D d_0)^{1/2}}\left(1-\frac{1}{\nu}\right)^{1/2}, \tag{8}$$

where R stands for the tip radius. We note that, in this relation, d_0 and V_c are implicitly parametrized by the tip temperature, i.e., the tip undercooling Δ: $d_0 = d_0(\Delta)$, $V_c = V_c(G,\Delta)$.

Some qualitative features of this theory are presented below. The first two agree with the experiment, the third questions the qualitative consequences of noise, and the latter conflicts with our observations:

(i) For fixed tip radius R and tip undercooling Δ (i.e., fixed d_0 and V_c), the noise amplification theory explains the destabilizing effect of V: $(\partial\Gamma/\partial V)_{\Lambda,G,R,\Delta} > 0$ from relation (8). This refers to the fact that, according to the planar instability, increasing front velocity promotes instability. It also suggests a similar effect of Λ, $(\partial\Gamma/\partial\Lambda)_{V,G,\Delta} > 0$, which might simply come from an increase of R with Λ. In such a case, at a given V and G, the net growth time of perturbations would be enhanced, not by an increase of the local growth rate σ of instability, but by a decrease of the tangential advection following a flattening of the tip.

(ii) The dispersion relation (6) shows that the driving force of the instability, i.e., the positive term $q(V-V_c)\mathbf{z}\cdot\mathbf{n}$ of the right-hand side, vanishes in the grooves together with $\mathbf{z}\cdot\mathbf{n}$. This is mainly due to the fact that the front normal velocity $V\mathbf{z}\cdot\mathbf{n}$ goes to zero as the grooves become parallel to the pulling velocity, so that the front then turns locally stable with respect to the planar instability. This implies that sidebranching should restabilize in the grooves, as observed experimentally [Figs. 5(a), 8(a)]. We note that this restabilization requires going beyond the circular approximation of the interface and is thus not contained in relation (8). On the other hand, as it relies on geometrical arguments, it also applies to confined free growth or to Saffman-Taylor growth [4].

(iii) As perturbations are considered to be in a linear growth regime, they only involve amplitude growth and no phase dynamics. Accordingly, the phase relations displayed by sidebranches should simply be those involved in the tip perturbations some time earlier. As these perturbations are supposed to result from thermodynamic fluctuations, sidebranches should thus be as uncorrelated as the thermal noise. At first sight, this does not seem in agreement with our observation (Figs. 1 and 4).

(iv) The variable λ_s in relation (8) recalls that the origin of sidebranching is, according to this theory, an instability of the tip mimicking the primary instability of a planar front. In this framework, the source of sidebranching instability can only follow the physics of the planar instability: increasing the thermal gradient weakens the growth factor, as confirmed by the decrease of $(1-1/\nu)$ with G in relation (8) at otherwise unchanged variables: $(\partial\Gamma/\partial G)_{V,\Lambda,R,\Delta} > 0$. As this conflicts with our indirect evidence of a destabilizing nature of G, we turn our attention below to other factors that may help solve this contradiction.

D. Destabilizing nature of the thermal gradient

In the planar instability, the thermal gradient is stabilizing since, for a given perturbation, increasing G with otherwise unchanged parameters reduces the undercooling and thus the growth rate of instability. Evidence of a destabilizing effect of G regarding the sidebranching instability thus indicates that its physics involves more than the usual instability mechanism of planar fronts. This is why a contradiction arises with the noise amplification theory when the thermal gradient is seen as only affecting the growth rate of the planar instability at the tip. Resolving it implies either changing the theoretical framework or considering other kinds of influence of the thermal gradient.

The first approach might involve considering other instability regions than the tip [2], other regimes than that pertaining to the WKB approximation [32], or other mechanisms such as those relying on a nonlinear global mode [33]. The second approach might consider the effect of the thermal gradient on the tip undercooling Δ or on the tip radius R. The former effect would modify the instability rate at the tip as considered in stability criteria based on local constitutional supercooling [28] and the latter would yield a different advective velocity and thus a different growing time for per-

turbations. Exploring them goes beyond the scope of the present paper.

E. Coherence and global mode

In the vicinity of the transition to sidebranching, sidebranch emissions occur by bursts [Figs. 5(a), 8(a)]. Farther from the onset, modulations of cell form are continuous in time, periodic, but weakly coherent. Finally, in the nonlinear regime where sidebranching amplitudes saturate in the grooves, sidebranches sometimes show a spatial and temporal regularity over typical spatial or temporal lengths as large as ten cells or ten cycles. This can be seen on sidebranching modes by the periodicity of the groove modulations observed on the whole front at a definite time [Figs. 1, 4(c)]. For some unknown reason, the phase order is eventually destroyed by the emission of a phase defect at cell tip [Fig. 4(a)]. The fact remains, however, that the instability modes show a tendency to synchronism that points to a phase-locking mechanism applying to different cells for each mode and to different periods for each cell. One possibility would be that sidebranches themselves induce perturbations to which the tip is sensitive. Then the system would become a closed loop. In such a case, its features would result from a competition between the direct effect of noise and the indirect effect of the feedback. As is well known, the latter might likely have dramatic consequences on system behavior.

To illustrate the above statement, we simply address sidebranching in a minimal model involving the basic ingredients discussed here: instability with noise and feedback. Taking time delays into account, the feedback loop would yield a model for the phase dynamics of sidebranches but its relevance would rely on specific discussions that go beyond the scope of the present analysis. We thus prefer to restrict our attention here to sidebranching amplitudes. According to this crude model, implemented in the Appendix, they would follow the noise level linearly for weak feedback but would be independent of noise for large ones. This shows that the nature of sidebranching may be deeply modified by feedback from sidebranches to the cell tip. More generally, nonlinear feedback might produce global modes, as recently shown in the context of hydrodynamical wakes [33]. Then, the system would have bifurcated from a noise amplifier regime to an oscillator regime.

VI. CONCLUSION

We have experimentally revisited the sidebranching transition of cells in directional solidification. A great deal of attention has been given to determining sidebranching features beyond the statistical level, by focusing attention to their dependence on single-cell spacings rather than on the average value of spacing over undetermined spacing distributions. This approach has been made possible by an accurate selection of the crystalline orientation over a large part of the sample. It enabled us to characterize the sidebranching of a given cell through those displayed by an assembly of equivalent cells. Meanwhile, it enabled the accuracy of the study to be enhanced by avoiding spurious spatiotemporal effects induced by pattern defects, anisotropy, or coupling between cells of different sizes.

Two sidebranching modes, referring to different crystalline orientations, have been identified. Their physical equivalence shows that sidebranching refers to a framework simpler than expected: it is independent of boundary conditions, involves weak mode couplings, and essentially corresponds to a two-dimensional phenomenon. The transition to sidebranching has been identified by reference to an order parameter, the sidebranching amplitude, and has been scanned with respect to pulling velocity, thermal gradient, and cell spacing. In the control parameter space, the critical surface of sidebranching shows neither fold nor singularity. This tends to reject the possibility of a bifurcation of the branch of solution as an origin of sidebranching.

The collapse of the critical surface determined by a scaling law reveals a destabilizing influence of the thermal gradient that conflicts with the basic features of the primary instability of planar fronts. This indicates that sidebranching includes *other* essential ingredients than the planar instability. These may include the evolution of tip undercooling or of the tip radius with the control parameters.

Altogether, these results show the need either for improving the noise amplification theory to account for the actual features of sidebranching in directional solidification or for investigating other kinds of instability mechanisms. These could stress other instability regions than cell tips or different interactions in the growth system, thereby yielding the possibility of a transition to a global mode for sidebranching.

ACKNOWLEDGMENTS

We thank B. Billia, A. Karma, P. Pelcé, P. Oswald, and S. de Cheveigné for stimulating discussions, and J. Minelli for technical assistance. This work was supported by the CNES and the CNRS.

APPENDIX

We address sidebranching amplitude within a minimal model involving noise amplification and feedback. We thus relate its value A at a given location to its value at the tip A_t through an amplification factor, labeled e^{Γ} in agreement with relation (5). Here A_t will be assumed to result not only from the noise amplitude η but also from a feedback F. Leaving aside the problems of time delay, we relate F to A: $F \equiv F(A)$. Moreover, in the spirit of a Landau expansion not involving the $A \rightarrow -A$ symmetry, we restrict ourselves to the form $F(A)=\varepsilon A-\mu A^2$ where ε and μ, positive, stand for feedback and saturation, respectively. We obtain

$$A = e^{\Gamma} A_t , \tag{A1}$$

$$A_t + \varepsilon A - \mu A^2 + \eta . \tag{A2}$$

The solution of this system gives $A=[B+(B^2+\eta\mu)^{1/2}]/\mu$ where $2B=\varepsilon-e^{-\Gamma}$. We consider that noise and saturation are sufficiently weak with respect to amplification so that $\eta\mu e^{2\Gamma}<1$. In a weak feedback regime, i.e., $\varepsilon e^{\Gamma}<1$, we obtain a sidebranching amplitude $A \approx \eta e^{\Gamma}$, di-

rectly dependent on the noise amplitude (Fig. 16). This is in agreement with the noise amplification theory. In a large feedback regime, i.e., $\varepsilon e^{\Gamma} > 1$, the model yields a sidebranching amplitude $A \approx \varepsilon/\mu$, independent of the noise amplitude and controlled by intrinsic variables of the system, ε and μ, only (Fig. 16). This is in qualitative disagreement with the noise amplification theory. The nature of sidebranching thus depends here on the level of feedback in the system.

[1] M. C. Cross and P. C. Hohenberg, Rev. Mod. Phys. **65**, 851 (1993).

[2] B. Billia and R. Trivedi, *Handbook of Crystal Growth* (Elsevier Science Publishers, Amsterdam, 1993), Vol. 1, Chap. 14.

[3] W. Kurz and R. Trivedi, Acta Metall. Mater. **38**, 1 (1990).

[4] P. Pelcé, *Dynamics of Curved Fronts* (Academic Press, New York, 1988).

[5] C. Huang and M. E. Glicksman, Acta Metall. **29**, 701 (1981).

[6] J. H. Bilgram, M. Firmann, and E. Hürlimann, J. Cryst. Growth **96**, 175 (1989); Ph. Bouissou, A. Chiffaudel, B. Perrin, and P. Tabeling, Europhys. Lett. **13**, 89 (1990); R. Trivedi and J. T. Mason, Metall. Trans. A **232**, 235 (1991).

[7] A. Dougherty, P. D. Kaplan, and J. P. Gollub, Phys. Rev. Lett. **58**, 1652 (1987); A. Dougherty and J. P. Gollub, Phys. Rev. A **38**, 3043 (1988).

[8] U. Bisang and J. H. Bilgram, Phys. Rev. Lett. **75**, 3898 (1995); Phys. Rev. E **54**, 5309 (1996).

[9] P. Molho, A. J. Simon, and A. Libchaber, Phys. Rev. A **42**, 904 (1990).

[10] M. A. Eshelman, V. Seetharaman, and R. Trivedi, Acta Metall. **36**, 1165 (1988).

[11] K. Somboonsuk, J. T. Mason, and R. Trivedi, Metall. Trans. A **15**, 967 (1984).

[12] F. Heslot and A. Libchaber, Phys. Scr. **T9**, 126 (1985).

[13] P. Kurowski, C. Guthmann, and S. de Cheveigné, Phys. Rev. A **42**, 7368 (1990).

[14] X. W. Qian and H. Z. Cummins, Phys. Rev. Lett. **64**, 3038 (1990); L. M. Williams, M. Muschol, X. Qian, W. Losert, and H. Z. Cummins, Phys. Rev. E **48**, 489 (1993).

[15] B. Billia, H. Jamgotchian, and R. Trivedi, J. Cryst. Growth **106**, 410 (1990).

[16] P. Pelcé and P. Clavin, Europhys. Lett. **3**, 907 (1987).

[17] R. Pieters and J. S. Langer, Phys. Rev. Lett. **56**, 1948 (1986).

[18] J. S. Langer, Phys. Rev. A **36**, 3350 (1987).

[19] M. N. Barber, A. Barbieri, and J. S. Langer, Phys. Rev. A **36**, 3340 (1987).

[20] B. Caroli, C. Caroli, and B. Roulet, J. Phys. (France) **48**, 1423 (1987).

[21] Ya. B. Zel'dovich, A. G. Istratov, N. I. Kidin, and V. B. Librovich, Combust. Sci. Technol. **24**, 1 (1980).

[22] M. Ben Amar and E. Brener, Phys. Rev. Lett. **71**, 589 (1993); E. Brener, *ibid.* **71**, 3653 (1993).

[23] E. Brener and D. Temkin, Phys. Rev. E **51**, 351 (1995).

[24] P. Pelcé and A. Pumir, J. Cryst. Growth **73**, 337 (1985).

[25] P. Pelcé, Europhys. Lett. **7**, 453 (1988).

[26] D. A. Kessler and H. Levine, Mod. Phys. Lett. **2**, 945 (1988).

[27] E. A. Brener, M. B. Geilikman, and D. E. Temkin, Zh. Eksp. Teor. Fiz. **94**, 241 (1988) [Sov. Phys. JETP **67**, 1002 (1988)].

[28] J. D. Weeks and W. van Saarloos, Phys. Rev. A **42**, 5056 (1990).

[29] H. Honjo, S. Ohta, and Y. Sawada, Phys. Rev. Lett. **55**, 841 (1985).

[30] S. K. Sarkar, Phys. Lett. A **117**, 137 (1986).

[31] O. Martin and N. Goldenfeld, Phys. Rev. A **35**, 1382 (1987).

[32] P. Huerre and P. A. Monkevitz, Annu. Rev. Fluid Mech. **22**, 473 (1990).

[33] J. M. Chomaz, Phys. Rev. Lett. **69**, 1931 (1992); A. Couairon and J. M. Chomaz, *ibid.* **77**, 4015 (1996).

[34] A. Papapetrou, Z. Kristallogr. **92**, 89 (1935); G. P. Ivantsov, Dokl. Akad. Nauk SSSR **58**, 56 (1947).

[35] A. Karma and P. Pelcé, Phys. Rev. A **39**, 4162 (1989).

[36] P. Kopczynski, W.-J. Rappel, and A. Karma, Phys. Rev. Lett. **77**, 3387 (1996); M. Georgelin and A. Pocheau, *ibid.* **79**, 2698 (1997).

[37] J. D. Hunt, K. A. Jackson, and H. Brown, Rev. Sci. Instrum. **37**, 805 (1966).

[38] S. Akamatsu, G. Faivre, and T. Ihle, Phys. Rev. E **51**, 4751 (1995).

[39] The term dendrite has initially been coined in free growth but has since been extended to directional growth. We use it here to denote unstable cells in spite of the possible differences between the two phenomena.

[40] G. I. Barenblatt, *Similarity, Self-similarity and Intermediate asymptotics* (Consultants Bureau, New York, 1979); G. I. Barenblatt, *Dimensional Analysis* (Gordon and Breach, New York, 1987).

[41] J. Bechhoefer and A. Libchaber, Phys. Rev. B **35**, 359 (1987).